Dogan Uzusen
Mechatronics Engineering Program,
Faculty of Engineering and Natural Sciences,
Sabancı University,
Orhanli, Istanbul 34956, Turkey
e-mail: doganu@sabanciuniv.edu

Ebru Demir
Mechatronics Engineering Program,
Faculty of Engineering and Natural Sciences,
Sabancı University,
Orhanli, Istanbul 34956, Turkey
e-mail: ebrudemir@sabanciuniv.edu

Osman Yavuz Perk
Mechatronics Engineering Program,
Faculty of Engineering and Natural Sciences,
Sabancı University,
Orhanli, Istanbul 34956, Turkey
e-mail: yavuzperk@sabanciuniv.edu

Ozlem Oral
Biological Sciences and Bioengineering Program,
Faculty of Engineering and Natural Sciences,
Sabanci University Nanotechnology
Research and Application Center,
Sabancı University,
Orhanli, Tulza, Istanbul 34956, Turkey
e-mail: ozlemoral@sabanciuniv.edu

Sinan Ekici
Department of Urology,
Maltepe University Hospital,
Maltepe University,
Maltepe, Istanbul 34956, Turkey
e-mail: ekicimiami@yahoo.com

Mustafa Unel
Mechatronics Engineering Program,
Faculty of Engineering and Natural Sciences,
Sabancı University,
Orhanli, Istanbul 34956, Turkey
e-mail: munel@sabanciuniv.edu

Devrim Gozuacik
Molecular Biology, Genetics and
Bioengineering Program,
Faculty of Engineering and Natural Sciences,
Sabancı University,
Orhanli, Tuzla, Istanbul 34956, Turkey
e-mail: dgozuacik@sabanciuniv.edu

Ali Kosar[1]
Mem. ASME
Mechatronics Engineering Program,
Faculty of Engineering and Natural Sciences,
Sabancı University,
Orhanli, Istanbul 34956, Turkey
e-mail: kosara@sabanciuniv.edu

Assessment of Probe-to-Specimen Distance Effect in Kidney Stone Treatment With Hydrodynamic Cavitation

The aim of this study is to focus on the effect of probe-to-specimen distance in kidney stone treatment with hydrodynamic bubbly cavitation. Cavitating bubbles were generated by running phosphate buffered saline (PBS) through stainless steel tubing of inner diameter of 1.56 mm at an inlet pressure of ~10,000 kPa, which was connected to a 0.75 mm long probe with an inner diameter of 147 μm at the exit providing a sudden contraction and thus low local pressures. The bubbles were targeted on the surface of nine calcium oxalate kidney stones (submerged in a water pool at room temperature and atmospheric pressure) from three different distances, namely, 0.5 mm, 2.75 mm, and 7.75 mm. The experiments were repeated for three different time durations (5 min, 10 min, and 20 min). The experimental data show that amongst the three distances considered, the distance of 2.75 mm results in the highest erosion amount and highest erosion rate (up to 0.94 mg/min), which suggests that a closer distance does not necessarily lead to a higher erosion rate and that the probe-to-specimen distance is a factor of great importance, which needs to be optimized. In order to be able to explain the experimental results, a visualization study was also conducted with a high speed CMOS camera. A new correlation was developed to predict the erosion rates on kidney stones exposed to hydrodynamic cavitation as a function of material properties, time, and distance. [DOI: 10.1115/1.4030274]

Introduction

Hydrodynamic cavitation is the generation of vapor bubbles due to the sudden drop in pressure when a liquid flows through a constriction. As the channel diameter reduces significantly, velocity of the flow increases due to the conservation of mass and a sudden pressure drop is observed leading to low local pressures.

[1]Corresponding author.
Manuscript received March 21, 2014; final manuscript received March 19, 2015; published online July 16, 2015. Assoc. Editor: Rosaire Mongrain.

 Copyright © 2015 by ASME

Downloaded From: http://medicaldevices.asmedigitalcollection.asme.org/ on 11/13/2015 Terms of Use: http://www.asme.org/about-asme/terms-of-use

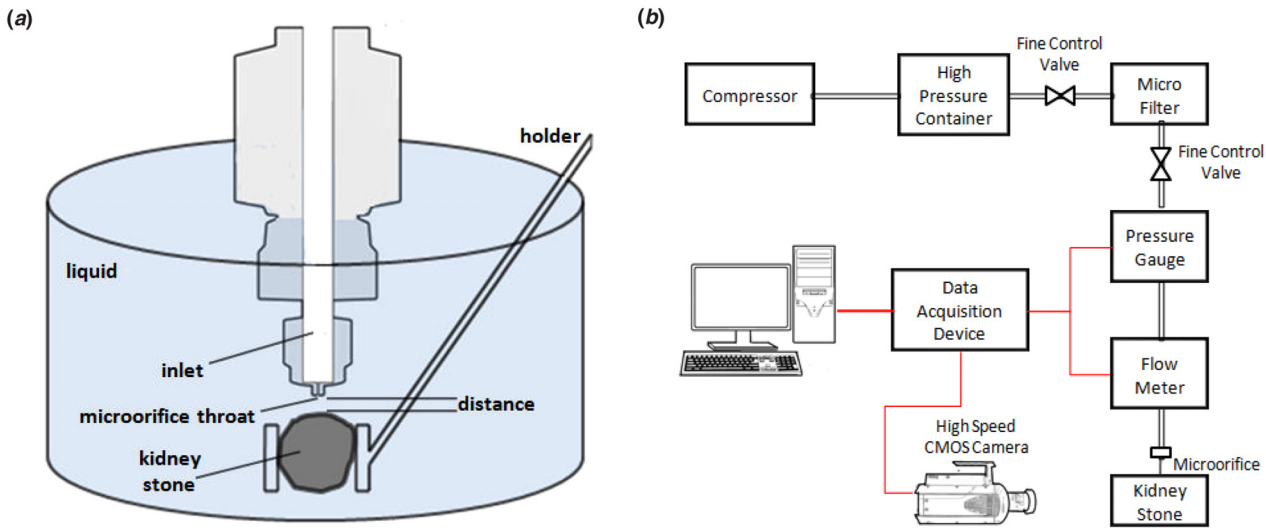

Fig. 1 (*a*) Microchannel configuration with the orifice throat and exit area and experimental placement of the kidney stone and (*b*) experimental setup

When the pressure drops to a critical pressure, cavitation inception occurs and bubbles start to be observed. When the emerging bubbles are exposed to atmospheric pressure, they collapse inward generating shock waves, which are of highly destructive nature for the exposed surfaces [1].

Cavitation in macroscale can be observed in ships' propellers and hydraulic turbines [2], which is typically considered as a phenomenon to be prevented and is a crucial design parameter for turbo machinery. However, the number of studies on exploiting the destructive nature of cavitating bubbles for various applications is continuously increasing. Jyoti and Pandit [3] showed that hydrodynamic cavitation is an energy efficient method for large scale water disinfection. Schneider et al. [4] used hydrodynamic cavitation to enhance boiling heat transfer of refrigerant R-123. Ji et al. [5] produced biodiesel with the help of hydrodynamic cavitation. Huang et al. [6] exploited the destructive effect of cavitating bubbles on degradation of chitosan to reduce its molecular size without changing its chemical structure. We have previously demonstrated that the destructive effects of hydrodynamic cavitation could be exploited to kill leukemia cells in in vitro culture [7] and in the ablation of benign prostatic hyperplasia tissues [8].

In our recent study, it is shown that hydrodynamic cavitation can successfully erode calcium oxalate kidney stones [9]. In fact, cavitation of ultrasonic origin has long been successfully used in kidney stone treatment by lithotripsy [10–13]. Ultrasonic procedures are noninvasive, yet, they have some limitations and side effects, including restrictions in the size, physicochemical properties, and location of stones to be treated [14–21]. Moreover, internal bleeding or severe pain during the passage of small stone particles through ureters and urethra may also be observed [22,23]. Application of ultrasonic cavitation to critical body parts other than kidney, such as eyes, breasts, and skin wounds, has its risks and limitations as well [21,24–26].

In addition to noninvasive extracorporeal shock wave lithotripsy, invasive techniques, ultrasonic lithotripsy, laser lithotripsy, or electrohydraulic lithotripsy with the aid of ureteroscopy are also present. The high price of the equipment for laser lithotripsy, accidental tissue injury, and ureteral perforation could be counted as the major disadvantages of laser lithotripsy. Moreover, not all calculi can be fragmented with one type of laser. Patients must be exposed to retreatment or additional clinical procedure to remove residual fragments [27]. The major disadvantage of electrohydraulic lithotripsy is the requirement of multiple maneuvers and prolonged hospital stay [28]. On the other hand, infections, nerve damage, internal bleeding, and ureteral injury may also be seen during the operation with instruments using ultrasound, laser, and electricity. Therefore, alternative techniques with less side effects and disadvantages should be developed and tested.

In our previous work, we reported the effects of hydrodynamic cavitation on kidney stone erosion and destruction for the first time [9]. In this work, we further focused on the dynamics of cavitation effects on kidney stones and searched for optimal destructive conditions. Here, we optimized the system and analyzed the effects of probe-to-specimen distance on erosion rate of kidney stones. The study was accompanied with extensive visualization tests conducted using a high speed camera. Monitoring microscopic images and processing them using several robust vision modules in the context of micromanipulation were carried out in our previous work [29–31]. Results presented in this work underline the importance of probe-to-specimen distance in exploiting the destructive nature of cavitating bubbles for biomedical applications, and provide a prediction tool for an average erosion rate as a function of probe to specimen distance and material properties.

Experimental Setup and Procedure

Experimental Setup. Experimental setup to generate cavitating bubbles was constructed based on the experimental setup used in Perk et al. [9], with the addition of piping extensions allowing the adjustment of the probe-to-specimen distance.

PBS contained in a high pressure vessel is propelled through a stainless steel tubing of an inner diameter of 1.56 mm at an inlet pressure of ~10,000 kPa (Fig. 1(*a*)). The inner diameter suddenly dropped to 147 μm at the exit due to the PEEK probe connected to the steel tubing with appropriate fittings, which acts as a microorifice. This orifice was submerged into a water tank, where the kidney stones were positioned at the desired distances relative to the orifice exit (Fig. 1(*a*)). Inlet pressure was monitored through a

Table 1 Material characterization of the calcium oxalate kidney stones [32]

Material	Kidney stone
Chemical composition	Calcium oxalate monohydrate
Density (g cm^{-3})	2.038
Young's modulus (GPa)	24.51
Shear modulus (GPa)	9.2
Poisson's ratio	0.33

Downloaded From: http://medicaldevices.asmedigitalcollection.asme.org/ on 11/13/2015 Terms of Use: http://www.asme.org/about-asme/terms-of-use

pressure gauge with 6.8 kPa sensitivity, while the flow rate was measured with a high pressure Omega turbine flow meter with 0.011 ml/s sensitivity (Fig. 1(*b*)). A control valve was used to adjust the flow rate.

The kidney stones were removed surgically at Maltepe University School of Medicine Hospital with the approval of Maltepe and Sabanci Universities' Ethics Committees. Their compositions were analyzed by X-ray diffraction (XRD). XRD results revealed that the kidney stones were composed of 90% calcium oxalate and 10% phosphate. Material properties of the kidney stones are already present in the literature [32] and are presented in Table 1.

In our experiments, we used a CMOS camera (Phantom v310, a trademark of Vision RESEARCH), which is a high speed camera with 10,000 frames per second. The speed of the camera is 3 Gpx/s and maximum speed at full resolution of 1280×800 (20 μm pixel size) is 3250 frames per second. The camera has a minimum frame rate of 24 fps. Blur can be eliminated and the minutest details can be seen by using short exposure times. On the v310, exposure time can be set to the minimum value of 1 μs. The camera supports 8- and 12-bit pixel depth. While smaller bit-depth implies more recording time and smaller files, greater bit-depth provides more gray levels and finer details. The greater digitalization of 12 bits facilitates acquiring more detailed data from the raw image.

Due to resolution and lighting issues, we used the camera at 3250 fps, which provides reasonably good images. The imaging system was equipped with two pulsed 198 high performance LED arrays having a total area of 180 mm $\times$ 120 mm and serving for background illumination. The average duration of the light pulses was approximately 60 μs, and the average time delay between the two consecutive images was tuned to 2 ms. We also utilized K2 DistaMax special lens, which offers ultimate in long-distance microscopy. TX tube of the lens provides 2$\times$ amplification in all cases, with all objectives, and with all working distance choices. It should be noted that although the Phantom v310 camera has sensitivity needed for even the most challenging lighting conditions, throughout our experiments, because of the insufficient lighting in the environment we utilized a variable iris in our camera system. Besides the focusing ring, the K2 DistaMax has a built-in iris diaphragm for depth of field and light attenuation control.

In order to obtain sharp images for efficient erosion detection, blur, which might occur in such microscopic images, must be removed. Blur could be the result of inappropriate imaging conditions such as out of focus camera, or relative motion of the camera and the imaged object. In order to remove or minimize the effect of the blur existing in the images, one can utilize a deblurring algorithm on the blurred images. Deblurring algorithms can be developed using either linear or nonlinear filtering approaches. In this work, we implemented a linear deconvolution type deblurring algorithm using image processing toolbox of MATLAB. Blurred images are deconvolved with a filter (mask), which has the size of $(2m+1) \times (2m+1)$ pixels, where m is an integer. In our implementations, we set $m=2$. The resulting enhanced images have sharper boundaries.

Experimental Procedure. After the experimental setup was prepared as explained above, PBS in the storage tank was pressurized and propelled into the stainless steel tubing and the probe, which is a PEEK microorifice of inner diameter of 147 μm. The cavitation number, σ, is a dimensionless number used for quantifying similar cavitating conditions and for representing the intensity of cavitation. The intensity of the cavitation was often described by the cavitation number, which is dependent on the local pressure at the orifice exit, vapor pressure of the liquid, flow velocity and the density of the fluid and is expressed as [33]

$$\sigma = \frac{(P_{ex} - P_v)}{\frac{1}{2}\rho V_{th}^2} \tag{1}$$

where P_{ex} is the exit pressure, P_v is the vapor pressure, ρ is the fluid density, and V_{th} is the flow velocity at the orifice. Since the inlet pressure determines the flow velocity, intensity of the cavitation is also dependent on the inlet pressure. Inlet pressure was increased, and cavitation inception was observed at a pressure of $\sim$483 kPa corresponding to a cavitation number of 0.35 with the emergence of bubbles from the probe exit consistent with the findings in the literature [33]. Due to the sudden pressure drop at the orifice, bubbly cavitation incepted leading to cavitating bubbles. The orifice exit was submerged in a water tank, where the kidney stones were positioned at a specified distance from the orifice exit. The emerging bubbles were exposed to ambient pressure at the exit of the probe, where the bubbles collapse occurred. Collapsing bubbles in the cavitating flow were targeted onto the kidney stone specimen surfaces so that the destructive effects of the collapse were exploited to erode the kidney stones.

Beyond cavitation inception, inlet pressure was further increase so that the flow rate was adjusted to 2 ml/s, while the flow velocity was 117.9 m/s at the orifice. The kidney stones were exposed to the cavitating flow with the corresponding cavitation number of 0.014 in this study at three different distances measured from the probe to specimen surface, namely, 0.5 mm, 2.75 mm, and 7.75 mm. In the light of the previous studies [7–9] of the authors, these three distances were chosen so that they could reveal the effect of the probe-to-specimen distance. The distance was adjusted with a home-made micromanipulator including a vision control system. Such manipulators based on compliant mechanisms are already present in the literature [29,34] and have resolutions of several micrometers. The distances were measured by inspecting the images taken with the camera based on the comparison with known dimensions in the system. This cavitation number was selected in parallel lines with the studies on microscale hyrodynamic cavitation and our previous study [9] to ensure erosion on the kidney stone sample surfaces. Each experiment was repeated for three different time durations, which were 5 min, 10 min, and 20 min. The probe–specimen distances were determined in the light of the images taken from visualization studies, which reveal the effective volume and range of emerging bubble

Table 2 Quantification of probe-to-specimen distance, application time, initial and final weights (mg) of the kidney stones, kidney stone erosion rates (mg and % min^{-1}) at 9790 kPa pressure

Specimen	Distance (mm)	Application time (min)	Initial weight (mg)	Final weight (mg)	Erosion rate (mg min^{-1})	Erosion rate (% min^{-1})
Stone 1	0.5	5	313.7	309.2	0.90	0.29
Stone 4	2.75	5	215	209.6	1.08	0.50
Stone 7	7.75	5	319.5	318.1	0.28	0.09
Stone 2	0.5	10	429.7	421.2	0.85	0.20
Stone 5	2.75	10	363.1	353.1	1	0.27
Stone 8	7.75	10	454.6	452.0	0.26	0.06
Stone 3	0.5	20	526.8	515.3	0.58	0.11
Stone 6	2.75	20	460.2	445.4	0.74	0.16
Stone 9	7.75	20	614.3	611.5	0.20	0.02

Downloaded From: http://medicaldevices.asmedigitalcollection.asme.org/ on 11/13/2015 Terms of Use: http://www.asme.org/about-asme/terms-of-use

clouds from the probe exit. The experimental matrix is presented in Table 2.

The mass of each kidney stone was measured before and after the experiments with an uncertainty of ±0.1 mg. The corresponding average erosion rates in mg/min were calculated by dividing the eroded mass by the evolved time. The percentage of erosion relative to the initial mass was obtained using the erosion amount, initial mass, and elapsed time. Sterile conditions were sustained by autoclaving all the probes, orifice throat, containers, and valves before each test. After each test, eroded kidney stones were placed to a sterile container kept at room temperature and were left for drying for a day. Thereafter, the weights of the specimens were measured again so that erosion amounts and rates could be assessed.

For assessing the erosional effects caused by hydrodynamic cavitation on kidney stones control experiments were performed. The control experiments were conducted with a probe having a larger inner diameter (∼2.8 mm). In these experiments, first of all, the same outlet velocities for both cavitating and noncavitating conditions were considered. For a small amount of time (∼5 min), no significant erosional change compared to a 5 min exposure to bubbly cavitating flow was observed in control experiments (noncavitating conditions) with the same outlet velocity.

The material of the kidney stones is the same for all samples according to the performed XRD results. The geometries are also similar so that no significant change in the surface morphology is expected for the samples. In addition, an additional test was also conducted as a control experiment similar to the work of Perk et al. [9]. Accordingly, a freely moving sample was exposed to bubbly hydrodynamic cavitation of the same density. The stone was confined but free to rotate. Under these conditions, the initial and final weights of the samples were also measured. The erosion on the samples had a similar trend for each case, and the change of the exposed area on the stones did not affect the total erosion amount on the exposed samples.

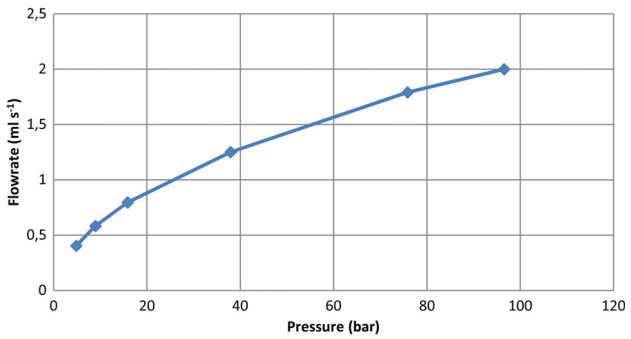

Fig. 2 Flow rate as a function of inlet pressure

Results

Figure 2 displays flow rate as a function of inlet pressure for bubbly cavitating flow conditions. The first data point corresponds to the cavitation inception condition, where cavitation number is around 0.35.

Due to approaching choking flow conditions, where an increase in flow rate and flow velocity would not be possible beyond a certain inlet pressure, the slope of the flow rate profile has a decreasing trend. Approaching choking conditions could be also recognized in Figs. 3–5.

Bubble clouds emerging from the test probe are displayed in Fig. 3. Bubble clouds were observed for three times using the same micro-orifice and flow conditions to check for the repeatability. No significant change in the cloud size and density was observed for each case. As seen from this figure, the bubble cloud has first a conical shape. The density of the cloud becomes lower as the distance from the probe is increased, which is due to the continuous collapse of bubbles, and thus, due to the continuous decrease in the number of bubbles in the bubble cloud as they move downstream the probe exit. After reaching the maximum cross section in the conical shape, the cross section of the bubble cloud has a decreasing trend, until all the bubbles collapse. As a result, it could be deduced that there is interplay between the intensity of bubble cloud and the bubble cloud cross section determining the exposed area, which is tabulated for different probe-to-specimen distances in Table 3. For a smaller probe–specimen distance, more bubbles can be targeted to a smaller exposed area with larger velocities.

Erosion amounts obtained from tested kidney stone samples are displayed as a function of time in Fig. 6. As can be observed in the figure, there exists an optimum probe–specimen distance in this study, namely, 2.75 mm, which provides the highest amount of erosion for all the application durations, which are 5.4 mg, 10 mg, and 14.8 mg for 5 min, 10 min, and 20 min of application, respectively. The lowest erosion amount is observed for the probe–specimen distance of 7.75 mm. This result indicates that

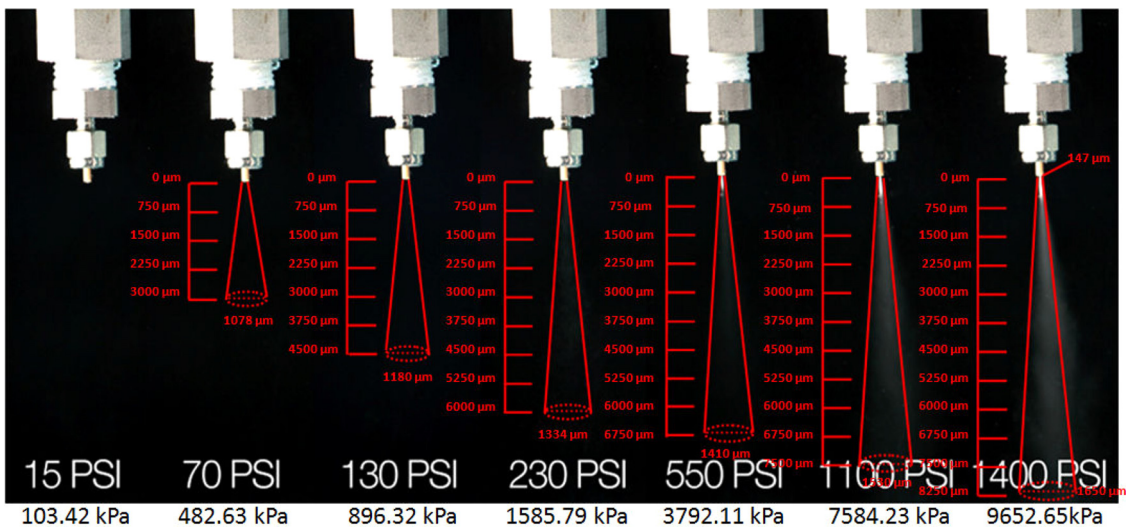

Fig. 3 Bubble cloud emerging from the probe exit at different cavitation intensities with assessment of effective range of bubbles and assessment of effective volume

Downloaded From: http://medicaldevices.asmedigitalcollection.asme.org/ on 11/13/2015 Terms of Use: http://www.asme.org/about-asme/terms-of-use

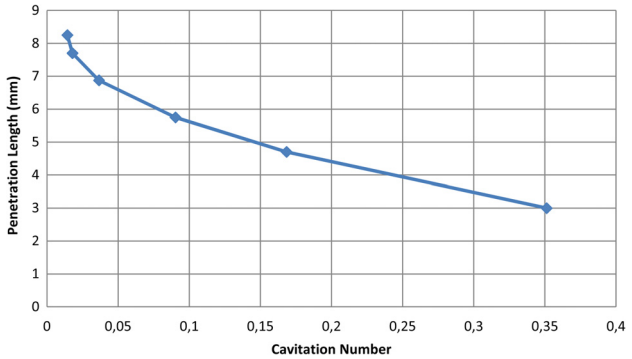

Fig. 4 Penetration length as a function of cavitationnumber

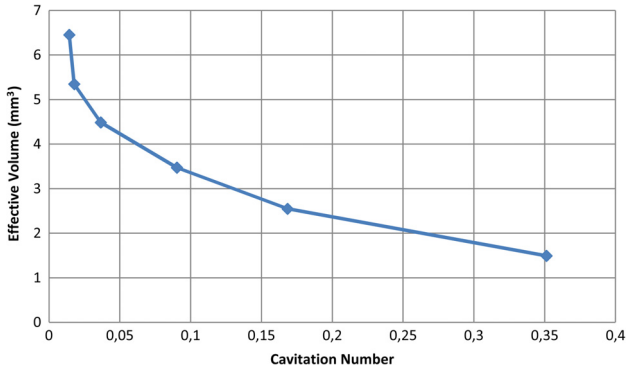

Fig. 5 Effective volume as a function of cavitation number

Table 3 Experimental kidney stone surface area which is exposed to erosion (mm^2) at 9790 kPa pressure for the probe–specimen distances of 0.5, 2.75, and 7.75 mm

Distance (mm)	0.5	2.75	7.75
Exposed area (mm^2)	0.045	0.33	1.91

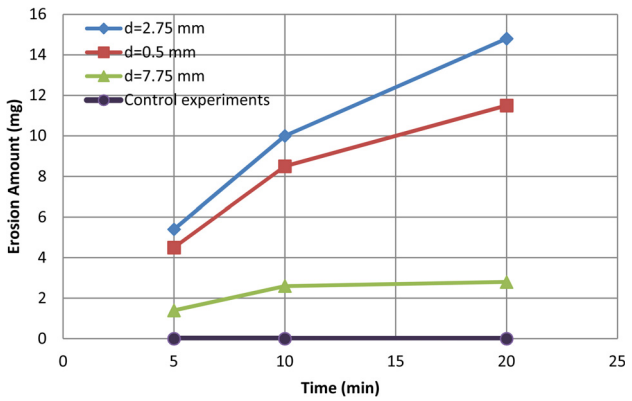

Fig. 6 Experimental results of kidney stone amount (mg) as a function of time (min) at 9790 kPa pressure for the probe–specimen distances of 0.5, 2.75, and 7.75 mm

the erosion rate induced by cavitating flows does not necessarily increase as the distance between the orifice and the specimen is reduced, but an optimum distance is present and should be determined, where the highest erosion amounts are attained. In order to explain this trend, visualization of cavitating bubbles for different distances from the probe was performed.

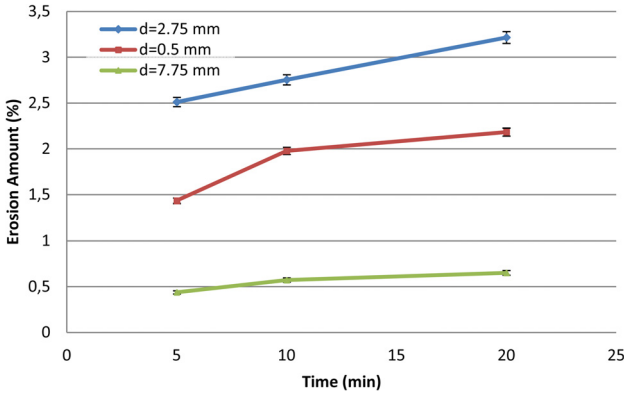

Fig. 7 Experimental results of kidney stone erosion rate (% min^{-1} with respect to the initial mass) as a function of time (min) at 9790 kPa pressure for the probe–specimen distances of 0.5, 2.75, and 7.75 mm

Erosion rates achieved throughout the experiments are presented in Table 2 and plotted in Fig. 7. The results have the same trends as the erosion amount results, which were averaged over the exposure time to obtain erosion rates. The highest average erosion rate is achieved at the distance of 2.75 mm (0.94 mg/min), whereas the lowest average erosion rate is found to be 0.25 mg/min at the distance of 7.75 mm. As it can be observed from Fig. 7, the erosion rate decreases with increasing application time.

Experimental erosion rate data in this study are used to develop a correlation providing the best prediction of the experimental data based on curve fitting using least squares method. This correlation is based on the approach of Crowe [1], where the erosion rate is written in terms of important parameter, which are R_p (in mm), the particle radius (average bubble radius, taken as 90 μm in this study), σ_b (in Pa), the flexural strength, E_t (in Pa), the Young's modulus of elasticity, t (in min), time, dis (in mm), probe–specimen distance, and is expressed as

$$W(\text{mg/min}) = 7074 \times 10^4 E_t^{0.8} \sigma_b^2 R_p^{-1.19}((-4.23) \times 10^{-11}\text{dis}^2 + (2.4) \times 10^{-10}\text{dis} - (1.01) \times 10^{-9})((4.22) \times 10^{-12} - (8.61) \times 10^{-14} t) \quad (2)$$

The above correlation can predict the experimental data with an MAE (mean absolute error) of 6.09%. All of the experimental data are within 25% of the correlation as shown in Fig. 8. Spherical particles are considered as bubbles, while it was also assumed that microbubbles emerging from the microprobe have the same velocity as the flow velocity inside the probe.

Discussion

The cavitation number corresponding to cavitation inception is in agreement with the cavitation inception numbers reported in the literature for microscale [4,33,35,36], while it is lower than cavitation inception numbers reported for macroscale [37,38], which is due to size scale effects. In contrast to stream nuclei observed in macroscale cavitation, surface nuclei are the key parameter for the inception of hydrodynamic cavitation in microscale, which is observed both in the literature and this study with the emergence of bubbles from the surface of the probe rather than from the bulk of the fluid. These differences are attributed to small residence time for surface nuclei and surface tension forces, which are significant at microscales [4,33,35,36]. Low incipient cavitation numbers were obtained from the experiments in microscale cavitation implying that cavitating flow conditions are more difficult to be attained in microscale, and there is a dominant size scale effect [33,35,36].

Downloaded From: http://medicaldevices.asmedigitalcollection.asme.org/ on 11/13/2015 Terms of Use: http://www.asme.org/about-asme/terms-of-use

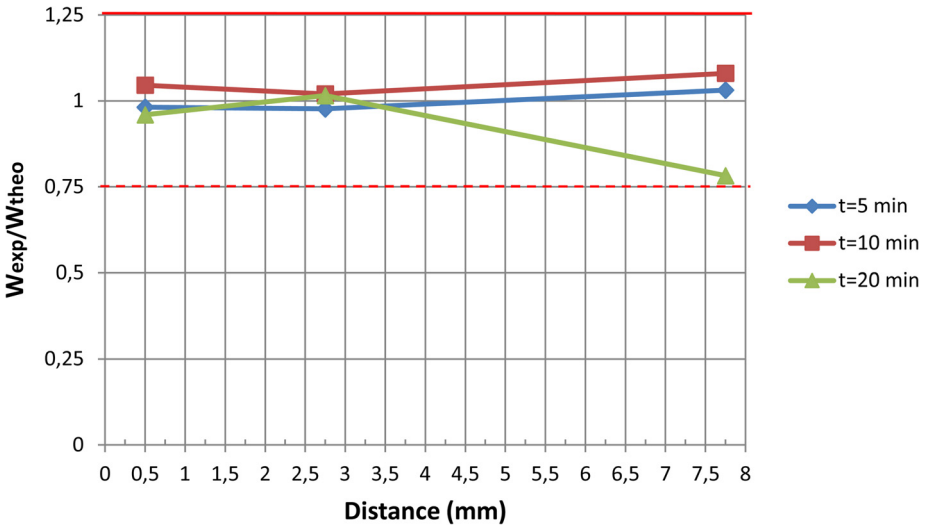

Fig. 8 Comparison of experimental erosion rate with predictions of the proposed correlation

The volume occupied by the bubble cloud (effective volume) grows with the decrease in cavitation number. However, the change in this volume becomes smaller and smaller because of the exponential trend with the applied inlet pressure implying that it is converging to a certain value. A similar trend is also valid for the effective range of the bubble cloud, which poses the limits of treatment with hydrodynamic cavitation at the same time. The maximum values for effective volume and effective range are 5.88 mm^3 and 8.25 mm, respectively, which are expected to be close to their maximum possible values. All these parameters are determined by processing the images by the camera system using the camera software. With the use of the software, the dimensions and important features can be easily assessed in detail. It can be also seen that bubbles emerging from the probe exit could reach to distances 56 times more than the inner diameter, and this value could serve for the limit for the probe–specimen distance.

Some of the hitting bubbles collapse when hitting the specimen, while the others bounce back from the specimen and collapse afterward. For a larger probe–specimen distance, fewer bubbles can be targeted to a larger exposed area with lower velocities due to the conservation of mass. Many bubbles collapse before hitting the target, and the effect of bubble collapse on the specimen diminishes with the distance. At an optimum distance, a large exposed area exists with a considerable hitting velocity of the bubbles, some of which already collapse at a close distance from the target, while the rest collapse after bouncing back from the specimen. Thus, there exists a maximum erosion amount at a fixed time for an optimum distance, which is 2.75 mm in this study. This result implies that a closer distance does not necessarily lead to a higher erosion rate, and the probe-to-specimen distance is a significant parameter affecting the erosion rate and should be optimized for a better erosion performance. The amount of erosion observed in the kidney stones increases with an increase in application time, which is in agreement with our previous findings [9].

The trends in Fig. 7 can be explained from scanning electron microscopy (SEM) images displayed in Fig. 9. Figure 9(*a*) shows an SEM image of the surface of an unexposed sample kidney stone sample with sharp edges on the surface, while Fig. 9(*b*) depicts the surface of an exposed kidney stone sample with destroyed edges. A significant difference in the unexposed stone's surface is present in the form of sharp points and crystal-like structures, which can be more easily removed with the exposure of bubbly cavitation, compared to the exposed kidney stone's surface. As can be observed, there is a gradual reduction in sharpness of the edges and corners with the cavitation exposure. A more "shaved-off surface," which is more difficult to be eroded, appears with increasing exposure time leading to a decrease in erosion rate with time.

Chemical composition of stones is also an important parameter for the erosion efficiency. Most of the kidney stones are composed of calcium and these stones, particularly calcium oxalate, are

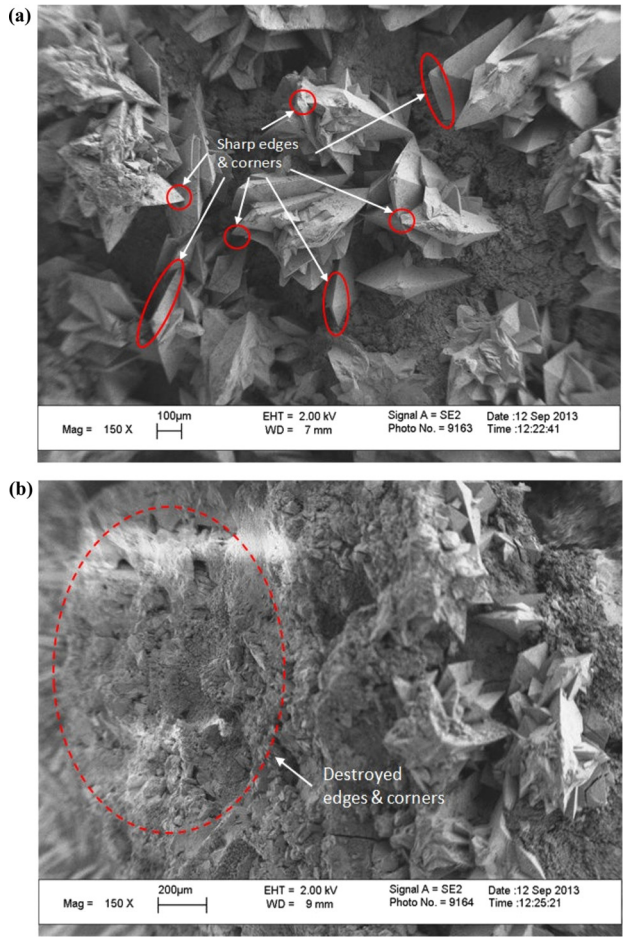

Fig. 9 (*a*) SEM image of an unexposed sample and (*b*) SEM image of exposed sample (exposed for 20 min at a probe–specimen distance of 2.25 mm)

Downloaded From: http://medicaldevices.asmedigitalcollection.asme.org/ on 11/13/2015 Terms of Use: http://www.asme.org/about-asme/terms-of-use

physically hard to destroy by conventional lithotripsy method. We have previously shown successful erosion of calcium oxalate kidney stones by hydrodynamic cavitation [9]. However, erosion efficiency may be limited for stones >0.5 cm in size. Although we have not tested the effect of hydrodynamic cavitation on softer stones such as uric acid or magnesium based stones, it is plausible that they may be eroded more easily. We are aware of the fact that usage of artificial stones could allow us to obtain data with lower variations and smaller standard deviations. Yet, even though natural stones were used in this study, we could obtain consistent and reproducible test results encouraging us about future clinical applications of the technique.

Conclusion

The findings of this study reveal the potential of using hydrodynamic cavitation in biomedical applications. Short application time required to erode and break the kidney stones, a potential to have less side effects because of easy probe targeting and manipulation possibilities, less heat generation at the target site and surroundings compared to ultrasound or laser-based techniques, and the simple yet effective methodology are proven to be some of the many advantages of using hydrodynamic cavitation in kidney stone treatment. Although in vivo animal experiments and clinical trials are yet to be done, in the light of data obtained from our previous work [7–9] and this study, we expect less side effects and complications such as kidney pelvis or ureter perforation, internal bleeding, tissue damage due to increased local temperature or infections using hydrodynamic cavitation. Since the efficiency was increased at optimal stone–probe distances, stones might be destroyed in a single session eliminating the need to use multiple interventions [9]. Further studies will reveal the in vivo performance and efficacy of the device.

In this study, the experimental setup is designed in a way that parameters such as probe-to-specimen distance, inlet pressure, and application time can be adjusted and optimized to increase the treatment efficiency, studies revealing the effects of changing abovementioned parameters are seen necessary. In this study, the effects of changing inlet pressure and changing probe-to-specimen distance are filtered out. Effects of changing the inlet pressure are observed via a visualization study using a high speed camera, whereas the kidney stones are subjected to hydrodynamic cavitation at different probe-to-specimen distances. Also, experiments are repeated for different application times, namely, 5, 10, and 20 min.

In the light of the presented data and results, the following conclusions are obtained:

- Different inlet pressures result in different penetration lengths (and accordingly different effective volumes), e.g., different maximum vertical distances measured from the probe, where cavitation effects can be observed.
- Probe-to-specimen distances studied in this work (0.5, 2.75, and 7.75 mm) are inside the range of the penetration length of the emerging bubble cloud, which is found to be 8.25 mm for a cavitation number of 0.014.
- This study shows that the probe-to-specimen distance is an important parameter to be optimized. The erosion rate increases with the distance up to an optimum value (2.75 mm), beyond which it has a declining trend.
- The maximum average erosion rate observed in this study is determined to be 0.94 mg/min at a 2.75 mm probe-to-specimen distance, whereas the minimum average erosion rate is 0.25 mg/min at a 7.75 mm probe-to-specimen distance.

A correlation to predict the erosion rate using probe-to-specimen distance, system parameters, and material properties as variables is developed, which could predict the experimental results with a mean absolute error of 6.09%. To amplify of the effect of the proposed method, multiple probes could be installed in parallel so that much higher erosion rates could be attainable. Since the size of such probes is rather small, such a configuration could easily fit in a regular endoscopy device. As a result, the proposed technique has a potential of providing much higher erosion rates with simple modifications and insertions in the system.

Acknowledgment

This work was supported by Sabancı University Internal Grant for Research Program under Grant Nos. IACF09-00642 and TUBITAK (The Scientific and Technological Research Council of Turkey) Support Program for Scientific and Technological Research Projects Grant Nos. 111M621 and 113S092. Undergraduate and graduate student support from Faculty of Engineering and Natural Sciences of Sabanci University and equipment utilization support from Sabanci University Nanotechnology Research and Applications Center (SUNUM) was also gratefully appreciated.

References

[1] Crowe, C. T., 2006, *Multiphase Flow Handbook*, CRC Press, Boca Raton, FL.
[2] Eisenberg, P., 1963, *Cavitation Damage*, Hydronautics, Washington, DC.
[3] Jyoti, K. K., and Pandit, A. B., 2001, "Water Disinfection by Acoustic and Hydrodynamic Cavitation," Biochem. Eng. J., **7**(3), pp. 201–212.
[4] Schneider, B., Kosar, A., and Peles, Y., 2007, "Hydrodynamic Cavitation and Boiling in Refrigerant (R-123) Flow Inside Microchannels," Int. J. Heat Mass Transfer, **50**(13), pp. 2838–2854.
[5] Ji, J., Wang, J., Li, Y., Yu, Y., and Xu, Z., 2006, "Preparation of Biodiesel With the Help of Ultrasonic and Hydrodynamic Cavitation," Ultrasonics, **44**(Suppl.), pp. 411–414.
[6] Huang, Y., Wu, Y., Huang, W., Yang, F., and e Ren, X., 2013, "Degradation of Chitosan by Hydrodynamic Cavitation," Polym. Degrad. Stab., **98**(1), pp. 37–43.
[7] Kosar, A., Sesen, M., Oral, O., Itah, Z., and Gozuacik, D., 2011, "Bubbly Cavitating Flow Generation and Investigation of Its Erosional Nature for Biomedical Applications," IEEE Trans. Biomed. Eng., **58**(5), pp. 1337–1346.
[8] Itah, Z., Oral, O., Sesen, M., Perk, O. Y., Erbil, S., Demir, E., Ekici, I. D., Ekici, S., Kosar, A., and Gozuacik, D., 2013, "Hydrodynamic Cavitation Kills Prostate Cells and Ablates Benign Prostatic Hyperplasia Tissue," Exp. Biol. Med., **238**(11), pp. 1242–1250.
[9] Perk, O. Y., Sesen, M., Gozuacik, D., and Kosar, A., 2012, "Kidney Stone Erosion by Hydrodynamic Cavitation and Consequent Kidney Stone Treatment," Ann. Biomed. Eng., **40**(9), pp. 1895–1902.
[10] Lingeman, J. E., McAteer, J. A., Gnessin, E., and Evan, A. P., 2009, "Shock Wave Lithotripsy: Advances in Technology and Technique," Nat. Rev. Urol., **6**(12), pp. 660–670.
[11] Weaver, J., and Monga, M., 2014, "Extracorporeal Shockwave Lithotripsy for Upper Tract Urolithiasis," Curr. Opin. Urol., **24**(2), pp. 168–172.
[12] Duryea, A. P., Roberts, W. W., Cain, C. A., and Hall, T. L., 2013, "Controlled Cavitation to Augment SWL Stone Comminution: Mechanistic Insights In Vitro," IEEE Trans. Ultrason. Ferroelectr. Freq. Control, **60**(2), pp. 301–309.
[13] Duryea, A. P., Roberts, W. W., Cain, C. A., Tamaddoni, H. A., and Hall, T. L., 2014, "Acoustic Bubble Removal to Enhance SWL Efficacy at High Shock Rate: An In Vitro Study," J. Endourol., **28**(1), pp. 90–95.
[14] Dretler, S., Pfister, R., Newhouse, J., and Prien, E., 1984, "Percutaneous Catheter Dissolution of Cystine Calculi," J. Urol., **131**(2), pp. 216–219.
[15] Klee, L. W., Brito, C. G., and Lingeman, J. E., 1991, "The Clinical Implications of Brushite Calculi," J. Urol., **145**(4), pp. 715–718.
[16] Zhong, P., Chuong, C. J., and Preminger, G. M., 1993, "Propagation of Shock Waves in Elastic Solids Caused by Cavitation Microjet Impact. II: Application in Extracorporeal Shock Wave Lithotripsy," J. Acoust. Soc. Am., **94**(1), pp. 29–36.
[17] Zhong, P., Chuong, C. J., and Preminger, G. M., 1993, "Characterization of Fracture Toughness of Renal Calculi Using a Microindentation Technique," J. Mater. Sci. Lett., **12**(18), pp. 1460–1462.
[18] Singh, I., Gupta, N. P., Hemal, A. K., Dogra, P. N., Ansari, M. S., Seth, A., and Aron, M., 2001, "Impact of Power Index, Hydroureteronephrosis, Stone Size, and Composition of the Efficacy of In Situ Boosted ESWL for Primary Proximal Ureteral Calculi," Urology, **58**(1), pp. 16–22.
[19] Coe, F. L., Evan, A. P., and Worcester, E., 2005, "Kidney Stone Disease," J. Clin. Invest., **115**(10), pp. 2598–2608.
[20] Kim, S. C., Matlaga, B. R., Tinmouth, W. W., Kuo, R. L., Evan, A. P., McAteer, J. A., Williams, J. C., Jr., and Lingeman, J. E., 2007, "In Vitro Assessment of a Novel Dual Probe Ultrasonic Intracorporeal Lithotriptor," J. Urol., **177**(4), pp. 1363–1365.
[21] Kim, S. C., Burns, E. K., Lingeman, J. E., Paterson, R. F., McAteer, J. A., and Williams, J. C., Jr., 2007, "Cystine Calculi: Correlation of CT-Visible Structure, CT Number, and Stone Morphology With Fragmentation by Shock Wave Lithotripsy," Urol. Res., **35**(6), pp. 319–324.
[22] Evan, A. P., Lynn, R. W., Bret, A. C., Trout, A., and Lingeman, J. E., 1996, "Renal Injury Induced by Clinical Doses of Shock Waves," J. Acoust. Soc. Am., **99**(4), p. 2510.
[23] McAteer, J. A., and Evan, A. P., 2008, "The Acute and Long-Term Adverse Effects of Shock Wave Lithotripsy," Semin. Nephrol., **28**(2), pp. 200–213.

Downloaded From: http://medicaldevices.asmedigitalcollection.asme.org/ on 11/13/2015 Terms of Use: http://www.asme.org/about-asme/terms-of-use

[24] Lingeman, J. E., Woods, J., Toth, P. D., Evan, A. P., and McAteer, J. A., 1989, "The Role of Lithotripsy and Its Side Effects," J. Urol., **141**(3 Pt 2), pp. 793–797.
[25] Evan, A. P., Willis, L. R., Lingeman, J. E., and McAteer, J. A., 1998, "Renal Trauma and the Risk of Long-Term Complications in Shock Wave Lithotripsy," Nephron, **78**(1), pp. 1–8.
[26] Evan, A. P., Willis, L. R., 2007, "Extracorporeal Shock Wave Lithotripsy: Complications," *Smith's Textbook on Endourology*, A. D. Smith, G. H. Badlani, D. H. Bagley, R. V. Clayman, and S. G. Docimo, eds., Decker, Hamilton, ON, Canada, pp. 353–365.
[27] Honeck, P., Wendt-Nordahl, G., Bolenz, C., Peters, T., Weiss, C., Alken, P., Michel, M. S., and Häcker, A., 2008, "Hemostatic Properties of Four Devices for Partial Nephrectomy: A Comparative Ex Vivo Study," J. Endourol., **22**(5), pp. 1071–1076.
[28] Lo, C. M., and Fan, S. T., 1991, "Percutaneous Transhepatic Choledochoscopic Electrohydraulic Lithotripsy for Common Bile Duct Stones: Experience in Four High-Risk Patients," Am. J. Gastroenterol., **86**(7), pp. 840–842.
[29] Bilen, H., and Unel, M., 2008, "Micromanipulation Using a Microassembly Workstation With Vision and Force Sensing," 4th International Conference on Intelligent Computing (ICIC 2008), Shanghai, China, Sept. 15–18, Vol. 5226, Vol. 5226, pp. 1164–1172.
[30] Bilen, H., Hocaoglu, M. A., Baran, E., Unel, M., and Gozuacik, D., 2009, "Novel Parameter Estimation Schemes in Microsystems," IEEE International Conference on Robotics and Automotion (ICRA'09), Kobe, Japan, May 12–17, pp. 2394–2399.
[31] Bilen, H., Hocaoglu, M., Unel, M., and Sabanovic, A., 2012, "Developing Robust Vision Modules for Microsystems Applications," Mach. Vision Appl., **23**(1), pp. 25–42.
[32] Heimbach, D., Munver, R., Zhong, P., Jacobs, J., Hesse, A., Mülles, S. C., and Preminger, G. M., 2000, "Acoustic and Mechanical Properties of Artificial Stones in Comparison to Natural Kidney Stones," J. Urol., **164**(2), pp. 537–544.
[33] Mishra, C., and Peles, Y., 2005, "Cavitation in Flow Through a Micro-Orifice Inside a Silicon Microchannel," Phys. Fluids, **17**(1), p. 013601.
[34] Acer, M., and Şabanoviç, A., 2013, "Micro Position Control of a 3-RRR Compliant Mechanism," IEEE International Conference on Industrial Technology (ICIT 2013), Cape Town, South Africa, Feb. 25–28, pp. 118–123.
[35] Mishra, C., and Peles, Y., 2006, "Development of Cavitation in Refrigerant (R-123) Flow Inside Rudimentary Microfluidic Systems," J. Microelectromech. Syst., **15**(5), pp. 1319–1329.
[36] Mishra, C., and Peles, Y., 2005, "Size Scale Effects on Cavitating Flows Through Microorifices Entrenched in Rectangular Microchannels," J. Microelectromech. Syst., **14**(5), pp. 987–999.
[37] Brennen, C. E., 1995, *Cavitation and Bubble Dynamics*, Oxford University Press, London.
[38] Brennen, C. E., 2005, *Fundamentals of Multiphase Flow*, Cambridge University Press, New York.

Downloaded From: http://medicaldevices.asmedigitalcollection.asme.org/ on 11/13/2015 Terms of Use: http://www.asme.org/about-asme/terms-of-use